3D phase field modeling of the morphology of WC grains in WC–Co alloys: The role of interface anisotropy

Han Li, Yong Du, Jianzhan Long, Zhijian Ye, Zhoushun Zheng, Helena Zapolsky, Gilles Demange, Zhanpeng Jin, Yingbiao Peng

Version of Record: https://www.sciencedirect.com/science/article/pii/S0927025621002536
Manuscript_f7d24f81bc30cb2e4d387e003ccc0e05

3D phase field modeling of the morphology of WC grains in WC–Co alloys: the role of interface anisotropy

Han Li[a], Yong Du[b,*], Jianzhan Long[c,*], Zhijian Ye[d], Zhoushun Zheng[d], Helena Zapolsky[f*], Gilles Demange[f], Zhanpeng Jin[a] and Yingbiao Peng[g]

[a]School of Materials Science and Engineering, Central South University, Changsha, Hunan, 410083, PR China

[b]State Key Laboratory of Powder Metallurgy, Central South University, Changsha, Hunan, 410083, PR China

[c]State Key Laboratory of Cemented Carbide, Zhuzhou, Hunan, 412000, PR China

[d]School of Mathematics and Statistics, Central South University, Changsha, Hunan, 410083, PR China

[f]GPM, UMR CNRS 6643, University of Rouen, 76575 Saint Étienne du Rouvray, France

[g]College of Metallurgical and Materials Engineering, Hunan University of Technology, Zhuzhou, Hunan, 412008, PR China

*Corresponding authors

E-mail: yong-du@csu.edu.cn (Yong Du); 281264623@qq.com (Jianzhan Long); Helena.zapolsky@univ-rouen.fr (Helena Zapolsky)

ABSTRACT

Understanding the morphological evolution of tungsten carbides (WC) grains is one of the few key factors to control the mechanical properties of the cemented carbides such as wear resistance and toughness. In this work, the three-dimensional (3D) equilibrium morphology of faceted WC grains in WC-Co system was prospected by means of phase-field simulations with parameters adjusted on ab-initio calculations. To model faceted grain surfaces, a specific class of high anisotropy functions harnessing the vertex vectors of the corresponding Wulff shape construction was implemented. As a result, both truncated trigonal prism in C-poor alloys, and trigonal prism in C-rich alloys in WC-25%Co system morphologies could be reproduced, depending on the magnitude of the anisotropy. Phase-field simulations show an excellent quantitative agreement with the present scanning electron microscopy (SEM) observations to representatively sintered WC-Co alloys. This approach paves a new way to model the morphology of high anisotropy grains.

Keywords: Phase-field model, facetted grain morphology, tungsten carbide, cemented carbides

Introduction

Tungsten carbides with a cobalt rich binder phase are among the most widespread cemented carbides[1]. This class of materials is characterized by a remarkable

combination of hardness, toughness and stability at elevated temperatures[2], whence their privileged use for drilling and cutting components[3]. The properties of cemented carbides are determined by their microstructural features, starting with the volume fraction and size distribution of hard phases[4]. Non-spherical shapes of solid grains such as the truncated trigonal or triangular prisms were observed in WC-Co alloys. The basal and prismatic facets of WC grains correspond to different crystal orientations, equipped with specific micro-mechanical properties[5]. In turn, the finest features of 3D faceted morphologies of WC grains such as their truncation and elongation factors[6] also influence the macroscopic mechanical performance of the material.[7-9] Therefore, understanding and predicting the detailed 3D morphology evolution of WC grains during material preparation is a strict prerequisite to upgrade mechanical properties of WC–Co alloys through optimized fabrication routes.

Cemented carbides are mostly manufactured by liquid phase sintering (LPS). During this process, solid faceted grains grow in the liquid binder phase. In WC-Co alloys, this growth was suggested to proceed by 2D nucleation/growth mechanism.[10-13] And yet, apart from a pioneering study of the anisotropic growth of WC grains in WC-25 wt. %–Co alloy by Ryoo et al[14] using the 2D pseudo-Monte-Carlo method, quantitative numerical models connecting the dots between anisotropic interface energy and the development of specific faceted morphologies of tungsten carbides hitherto remain scarce. Moreover, as far as we know, the experimentally observed prismatic shape of WC grains has not been simulated in three dimensions yet. In this work, we address the influence of the anisotropy of the interfacial energy on the

morphology development of faceted tungsten carbides grains in WC–Co cemented carbides, from both numerical and experimental perspectives.

A numerically efficient way to reproduce faceted morphologies at mesoscopic scale and connect it to the anisotropic surface energy is provided by the Phase-Field model (PFM).[15] This approach was notably used to study the formation of facets in Nickel thin films[16], ice dendrites[17, 18] and equilibrium voids under irradiation[19]. Now, most PFM rely upon regularization procedures to circumvent the numerical instability induced by faceting (seeing for instance in refs. [20-25]) resulting in the increase of the complexity and a potential loss of transferability for the implemented algorithms. We thus opted for an alternative faceting approach proposed in refs. [26] and [27], where the anisotropy function is defined directly from the equilibrium crystal shape (ECS). Not only this approach was proved to be stable without need for any regularization procedure, but also it directly connects the energy of facets to the anisotropy function in the PFM in a convenient way.

In this study, a 3-D phase field model for highly anisotropic interfacial energy is presented and the anisotropy functions are derived for WC grains. The model parameters are evaluated based on available data extracted from the ab-initio calculations. In parallel, WC-Co cemented carbides with different carbon contents were manufactured by LPS and the microstructure were observed by scanning electron microscopy. The simulation results are compared to the Wullf construction and our own experimental observations. The validity of the model is then discussed.

Results

The phase-field model

The shape relaxation of tungsten carbide grains is modeled under constant volume constraint. Based on the volume conservation of carbides, we assume that mass transport can be neglected. For this reason, it is not explicitly included in the model. Then only one variable φ referring to the phase matrix (φ=0) and solid phase particle (φ=1) is necessary to describe the kinetics of the shape relaxation of grains. The relaxation kinetics of the shape of the WC grain is governed by the Allen-Cahn (non-conserved) phase-field equation:

$$\frac{\partial \varphi}{\partial t} = -L\frac{\delta F}{\delta \varphi} \qquad (1)$$

where L is the kinetic coefficient and F is the total free energy of the system, defined as the integral of the free energy density f over the total volume of system. The energy density f for a heterogeneous system can be expressed in terms of φ and its gradient $\nabla\varphi$ as:

$$f(\varphi, \nabla\varphi) = \omega g(\varphi) + \frac{\varepsilon^2}{2}(\nabla\varphi)^2 + h(\varphi)\mu_p + \big(1 - h(\varphi)\big)\mu_m \quad , \qquad (2)$$

Here $g(\varphi)$ is the double-well function guaranteeing local minima at φ =0 and φ =1[28].

$$g(\varphi) = \frac{1}{4}\varphi^4 - \left(\frac{1}{2} - \frac{1}{3}m\right)\varphi^3 + \left(\frac{1}{4} - \frac{1}{2}m\right)\varphi^2, \qquad (3)$$

In ref. [28], the parameter m is used to introduce the driving force for grain growth and is set to 0 in our simulation.

The coefficient ω in Eq.(2) controls the height of energy barrier between two minima at a given temperature. The coefficient ε is the gradient energy coefficient. Following

the procedure proposed by Fleck et al[29], the term $h(\varphi)\mu_p + \big(1 - h(\varphi)\big)\mu_m$ imposes the conservation of the solid grain volume. Here, μ_p and μ_m are energy densities for bulk particle and matrix, respectively, and $h(\varphi) = \varphi^3(6\varphi^2 - 15\varphi + 10)$ is an interpolation function. Then, the evolution equation (1) can be further developed as:

$$\frac{\partial \varphi}{\partial t} = -L\left(\frac{\partial f}{\partial \varphi} - \nabla \cdot \frac{\partial f}{\partial(\nabla \varphi)} + h'(\varphi)\mu_0\right) \tag{4}$$

where the parameter $\mu_0 = \mu_p - \mu_m$ is set by the constraint of constant volume for the particle $\int_V \frac{\partial \varphi}{\partial t} dV = 0$ with respect to the following formula:

$$\mu_0 = \frac{\int_V \left(\nabla \cdot \frac{\partial f}{\partial(\nabla \varphi)} - \frac{\partial f}{\partial \varphi}\right) dV}{\int_V h'(\varphi) dV} \tag{5}$$

The value of μ_0 is evaluated dynamically at each time step.

The parameters of the phase-field model, namely ω, ε, and L in Eqs. (2) and (4) can be linked to the interface properties of the system, such as the interface thickness ξ, the interfacial energy σ and the interface mobility M:

$$\xi = \sqrt{\frac{2}{w}}\alpha\varepsilon \tag{6}$$

$$\sigma = \frac{\varepsilon\sqrt{w}}{6\sqrt{2}} \tag{7}$$

$$M = \frac{12L\varepsilon}{\sqrt{2w}} \tag{8}$$

Note that M is defined as the interface velocity driven by a unit of driving force, so its value is independent of the parameter m.

The modelling of the faceted morphology of WC grains is performed via the specification of the anisotropic interfacial energy. For that purpose, we posit that the gradient coefficient ε depends on crystal orientation:

$$\varepsilon = \varepsilon_0 f_{aniso} \tag{9}$$

Here, ε_0 is the gradient coefficient in the isotropic case and f_{aniso} is the anisotropy function. Typically, f_{aniso} depends on the normal vector $\vec{n} = \frac{\nabla\varphi}{|\nabla\varphi|}$ to the interface. From Eq.(7), the interfacial energy thus becomes:

$$\sigma = \frac{\varepsilon_0\sqrt{w}}{6\sqrt{2}} f_{aniso} = \sigma_0 f_{aniso} \tag{10}$$

where σ_0 can be regarded as the average interfacial energy of the system.

The salient ingredient for the reproduction of carbides faceted morphology is the expression of the anisotropy function f_{aniso}, introduced in Eqs. (9) and (10). In most PFM, the anisotropy function is chosen to account for the crystalline symmetry, using combinations of trigonometric[17, 18, 30, 31] or spherical harmonic[19] functions, weighted by anisotropy parameters. Above a certain threshold value for the anisotropy parameters, a range of crystal orientations become unstable and faceting can be achieved, at the price of the instability of the numerical scheme. This problem is then solved by adding higher order terms to the surface energy[20, 23, 25], by convexifying the inverse polar plot of the anisotropy function[32], or by just-so removing the cusps in the anisotropy function[21]. The first approach involves the addition of a curvature-dependent regularization term to the energy density expression. Hence extra calculation of mean curvature and evaluation of the regularization parameter are needed. The last two approaches involves the replacement of the anisotropy function near the cusps by regularized or smoothed functions. Such treatment may become complex for a 3D problem. Due to their substantial computational cost and complexity, we suggest that the referred procedures are not best indicated for the dynamics of faceted particles relaxation. The class of anisotropy functions introduced

in ref. [26] and [27] was then used in this work. These functions are defined piecewise by: $f_{aniso}(\vec{n}, \vec{\eta}_k) = \underset{1 \le k \le m}{max} \{\vec{n} \cdot \vec{\eta}_k\}$, where $\vec{\eta}_k$ is the k_{th} vertex vector of the shape of the crystal grain, itself connected to the interface energy. For the typical shapes of a WC grain, the vertex vectors $\vec{\eta}_k$ are shown in fig.1a and fig.1b. The construction of the anisotropy function from the vertex vectors is sketched in two dimensions for a truncated triangle in Fig. 1c. In the present work, the anisotropy functions constructed from Fig.1a and Fig.1b are referred to as types I and II respectively.

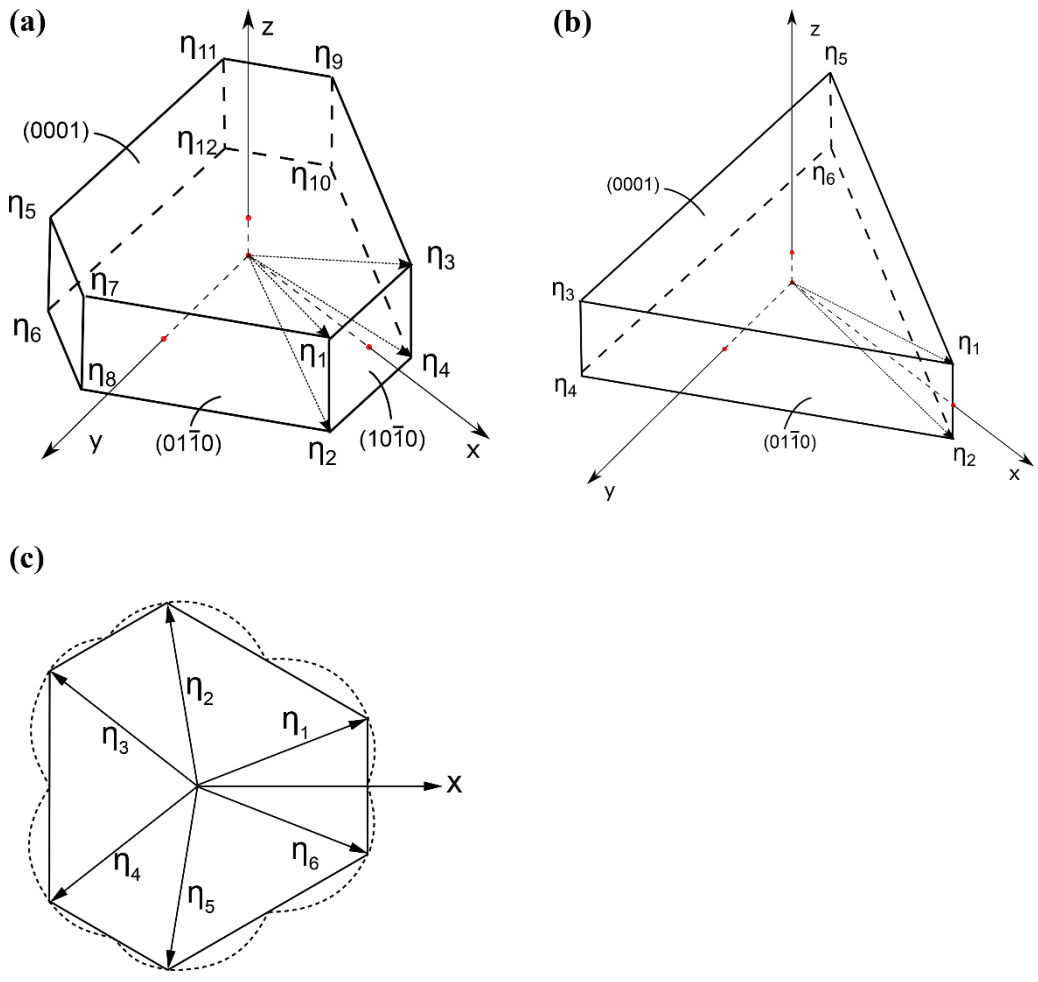

Fig.1 Schematic illustration of η vectors for (a) truncated trigonal prism, (b) triangular prism and (c) the polar plot of anisotropy function (dotted line) constructed from a truncated triangle.

Assessment of the material properties

According to Su et al's work[33], the WC grains appear as irregular laminar structure after ball milling, and change to multi-faceted shape during subsequent sintering. Therefore, the WC/Co interfacial energy should be considered. Interfacial energy for each facet of WC is difficult to measure experimentally. In this work, 3 simulation cases (listed in Tab.1) were set based on the ab-initio calculations from Christensen et al's work[34, 35]. Case 1 and Case 2 correspond to C-poor and C-rich conditions in the ab-initio calculations, respectively. In both cases, the ECS for WC grains is the truncated trigonal prism (see next section) and type I anisotropy function was used. In case 3, we aimed at reproducing the triangular prism, often observed experimentally in C-rich alloys. Then type II anisotropy function was used. The input values of $\sigma_{(0001)}$ and $\sigma_{(01\bar{1}0)}$ were the same as Case 1 while $\sigma_{(10\bar{1}0)}$ was fixed to $2\sigma_{(01\bar{1}0)}$ to make this orientation energetically unfavorable.

Tab.1 Interfacial energy data used in simulation

	Interfacial energy (J/m^2)			Type of f_{aniso}
	$\sigma_{(0001)}$	$\sigma_{(01\bar{1}0)}$	$\sigma_{(10\bar{1}0)}$	
Case 1	1.52[35]	1.80[34]	2.85[34]	I
Case 2	1.73[35]	1.94[34]	3.14[34]	I
Case 3	1.52[35]	1.80[34]	3.60[this work]	II

The expressions of σ are determined from Tab.1. The interface width ξ=5×10^{-7} m was adopted from ref.[36] and the value of α in eq.7 was chosen to be 2.2. The value for L was set to $5 \times 10^{-10}\, m^3/(J \cdot s)$, so that the mobility of (0001) interfaces $M_{(0001)}$was $1.16 \times 10^{-15}\, m^4/(J \cdot s)$ for Case 1 and $1.20 \times 10^{-15}\, m^4/(J \cdot s)$ for Case 2, in agreement with the value in ref. 10 (which is $1.0 \times 10^{-15}\, m^4/(J \cdot s)$).

Shape relaxation for single WC grain

The interfacial anisotropy model is first checked against theoretical prediction of equilibrium shape (ECS). Generally speaking, the Wulff construction allows to determine the equilibrium shape of an isolated crystal from the polar plot of its interfacial energy.[37] An alternative way to assess the equilibrium morphology of a crystal in 3-D case involves the ξ-vector formalism proposed by Hoffman and Cahn[38]. The ξ-plot is similar in shape to the Wulff construction, albeit scaled by a factor.

Fig. 2 displays the polar plots of σ, 1/σ and the corresponding ξ-plots. The minima on the plots of σ correspond to vertices on the 1/ σ plots, indicating the stable interface orientations. As for other part of the σ plot, it should be regarded as an interpolation, so that the σ function as a whole still generates the equilibrium shape while concurrently keeping the 1/ σ plot convex. In a nutshell, the present model is a compromise between real properties of the grain and numerical stability of the simulation.

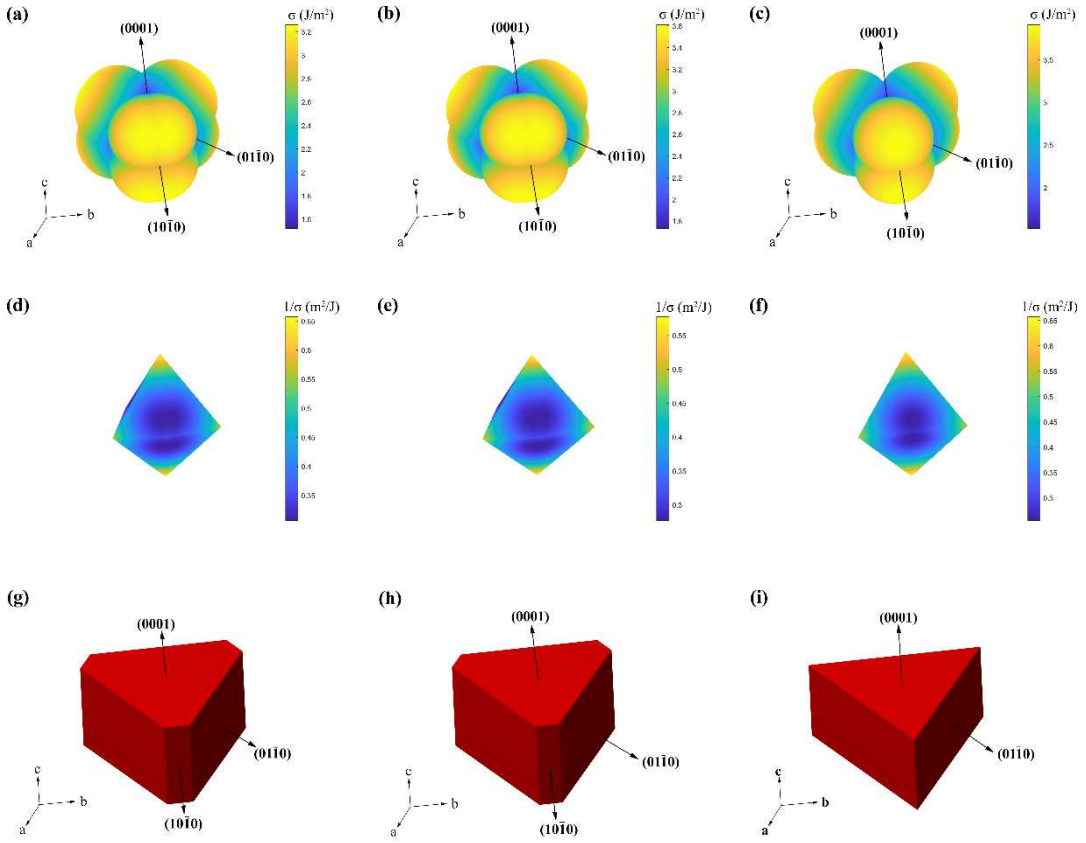

Fig.2 The plot of σ, $1/\sigma$ and the corresponding ξ-plot: the first column corresponds to Case 1, the second to Case 2 and the third to Case 3.

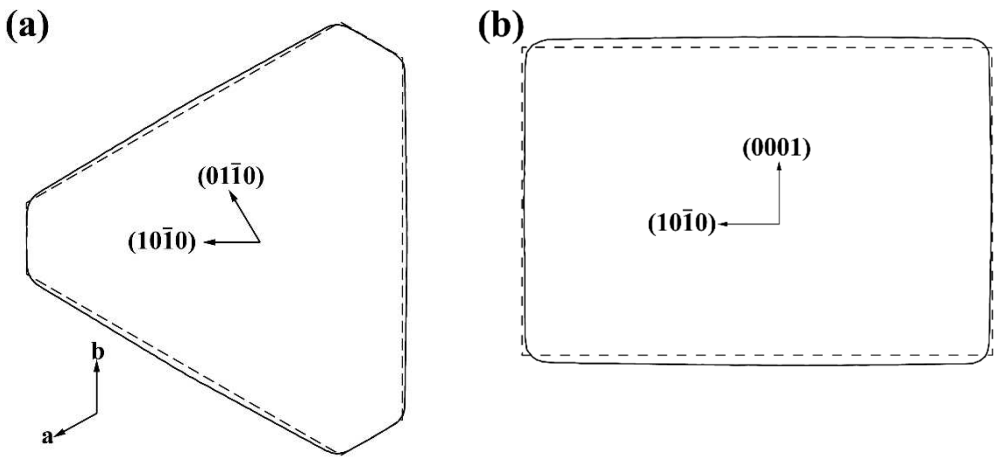

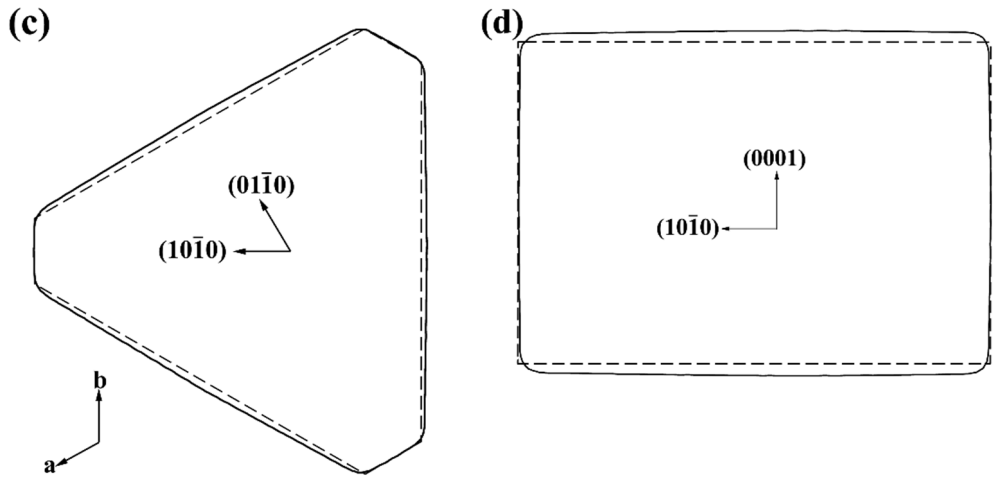

Fig.3 2D slices showing comparison between simulation (solid lines) and theoretical prediction (dashed line). (a) and (b): Case 1; (c) and (d): Case 2. The simulated morphologies contours plotted at φ=0.5.

According to the ξ-plots, the equilibrium shapes of WC grains for Cases 1 and 2 are both truncated trigonal prisms but slightly different in their shape factors. Fig.3 compares the simulated and the theoretically predicted morphologies for cases 1 and 2. The simulation accuracy is satisfactory given that no extra treatment is used to reduce numerical errors from discretization.

Figure 4 shows the experimental observation versus the grain shapes simulated by the phase-field model hereby developed. Figure 4(a) and (b) present the experimental morphology of WC grains in C-poor and C-rich alloys, respectively. In general the WC grains in the C-poor alloy are more truncated trigonal prisms, while those in the C-rich alloy are mainly triangular prisms. Step structures on the surface of some grains were also observed in the C-poor alloy. This result complies with the study of Kim et al[39]. Figure 4(c) and (d) show the simulated 3D WC grain for Cases 1 and 2.

Delanoë and Lay[6] have experimentally measured the shape factors of WC grains in WC-Co alloys after sintering. They suggested that in C-poor alloy with high Co content (22.5 wt.%) and sintered for long time (10 h at 1450 ° C), the shape of WC crystals can be regarded as at equilibrium. The corresponding truncation factor *r* and elongation factor *k* are 0.25 ± 0.02 and 0.82 ± 0.07 respectively. As a comparison, the resulting *r* and *k* factors are 0.21 and 0.70 respectively for Case 1 simulation. As previously discussed, upon using the available interfacial energy obtained by ab-initio calculation, phase-field simulations only generate truncated trigonal prisms as the equilibrium grain shape. To reproduce triangular prism, the energy gap between the 2 types of prismatic interfaces should be significant. This prerequisite matches Case 3 and the equilibrium shape of WC grain displayed in Fig.4(e).

Figure 5 shows the simulated shape relaxation process of a WC grain for Case 1. As the system minimizes its total energy, facets developed swiftly from the spherical grain. Then, a truncated prism consisting in facets with relatively low interfacial energy is formed. Finally, shape factors draw near their equilibrium values.

Discussion

The comparison between experimental observations and simulation results suggest that the shape of a fraction of grains presented in C-poor alloy relates to the middle stage of grain evolution. However, it should be noted that the simulated grain forms facets corresponding to {0001} and {10-10} planes of the WC crystal, while an extra type of facets is often observed in the prepared C-poor alloy . These facets are

supposed to be {10-11} planes according to measurements of Kim et al and Sugiyama et al's[39, 40]. In our simulations, only 3 types of interfaces have been considered. In order to account for more complex grain morphologies, the energy of {10-11} interfaces should also be evaluated and included in the model.

In real alloys, a large grain size distribution is observed, reflecting the process of grains growth phenomenon[11] . For example, the step morphology envisioned in some grains in the C-poor alloy provide a circumstantial piece evidence of this growth regime. The addition of this mechanism to the present model therefore appears as a necessary refinement to further unravel the host of WC grains' morphologies observed during growth.

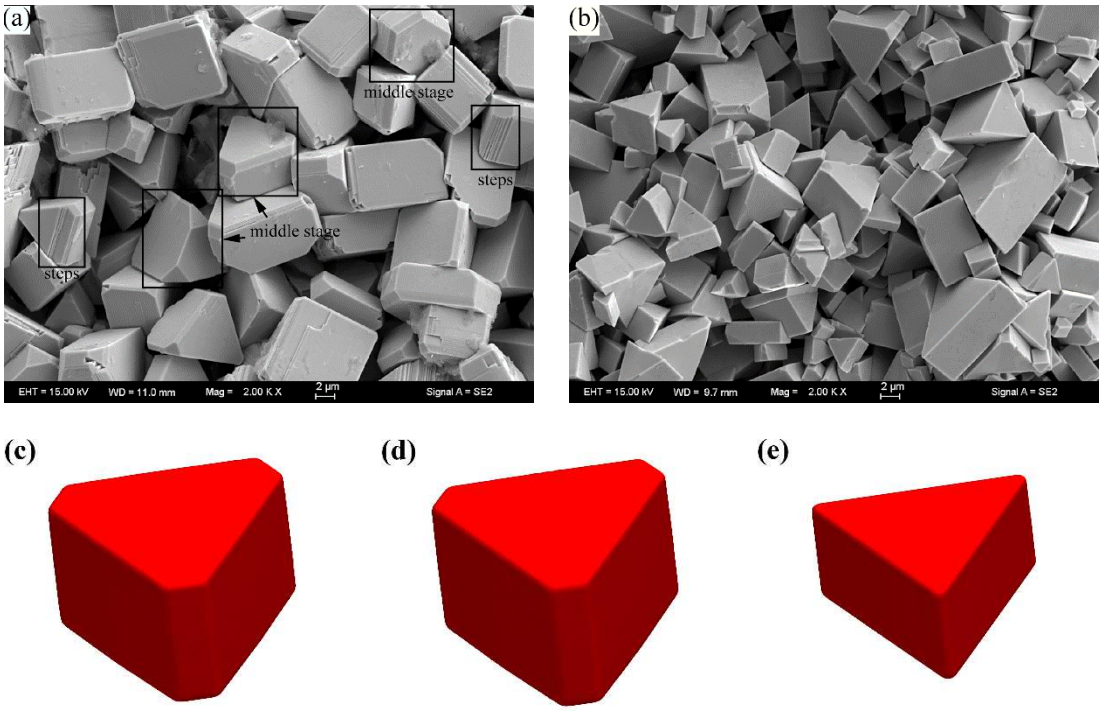

Fig.4 Experimentally observed WC grains in WC–Co hard metals: (a) C-poor alloy; (b) C-rich alloy and simulated equilibrium WC grain morphology for (c) Case 1, (d) Case 2 and (e) Case 3

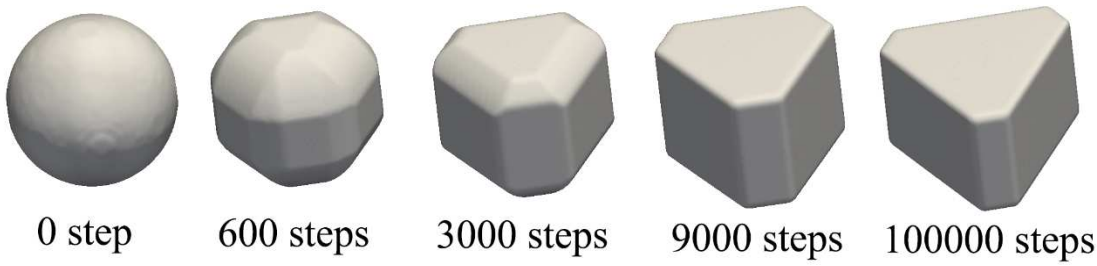

Fig.5 Simulated morphology evolution of a single WC grain for case 1 driven by shape relaxation

In summary, a 3-D phase field model equipped with anisotropic interfacial energy was developed to predict the shape evolution of WC grain in WC-Co alloys. Phase field results were first compared with theoretical calculations of equilibrium shape of WC grains, and secondly with the present experimental observations. It was concluded that the anisotropy of interfacial energy is a key parameter which determines the equilibrium shape of grains. The specific choice of the ratio between interfacial energy $\sigma_{(01\bar{1}0)}$ and $\sigma_{(10\bar{1}0)}$ allows to reproduce the evolution of grain shape from a trigonal prism to a truncated trigonal prism. The truncated triangular prism shape of WC grains was shown to be an equilibrium shape observed only in the C-poor WC–Co alloys, where $\sigma_{(01\bar{1}0)}/\sigma_{(10\bar{1}0)}$≈1.6. Besides, in the case of C-rich alloys, where $\sigma_{(01\bar{1}0)}/\sigma_{(10\bar{1}0)} \geq 2$, the trigonal prism morphology of WC grains could

be reproduced by phase field simulations and concurrently observed in experiments. The shape relaxation process obtained numerically is in a good agreement with experimental data and reproduces well the non-equilibrium shape of grains. We believe that the incorporation of an exhaustive dataset of interfacial energies spanning the different types of WC grains' interfaces in the phase field model opens a way to highly tunable models that could provide deep physical insights on grain morphology and growth in cemented carbides. The present simulation work provides insights on how interfacial energy may affect the evolution process of WC grains in WC-Co alloys and lays basis for more realistic models where the growth phenomena will be also taken into account.

Method

Modeling Method

The kinetic Eq. (4) was solved in dimensionless form

$$\frac{\partial \varphi}{\partial \tilde{t}} = -\tilde{L}\left(g'(\varphi) - {f_{aniso}}^2\tilde{\nabla}^2\varphi + 2f_{aniso}\tilde{\nabla}f_{aniso}\cdot\tilde{\nabla}\varphi + \frac{\partial}{\partial\tilde{x}}\left[\left(\tilde{\nabla}\varphi\right)^2 f_{aniso}\frac{\partial f_{aniso}}{\partial\varphi_{\tilde{x}}}\right] + \frac{\partial}{\partial\tilde{y}}\left[\left(\tilde{\nabla}\varphi\right)^2 f_{aniso}\frac{\partial f_{aniso}}{\partial\varphi_{\tilde{y}}}\right] + \frac{\partial}{\partial\tilde{z}}\left[\left(\tilde{\nabla}\varphi\right)^2 f_{aniso}\frac{\partial f_{aniso}}{\partial\varphi_{\tilde{z}}}\right]\right).$$

The volume conservation term is ommited here for simplicity. For a detailed evaluation of model parameters, please refer to the supplementary information.

The phase-field equation was solved using forward Euler time integration and central finite difference space discretization in a simulation box with uniform grid spacing and periodic boundary conditions.

Experiment method

An experimental study of WC grains growth under a host of carbon contents was conducted. The 25 wt.% binder content was selected for WC–Co alloys so as to reduce the influence of mutual contact between WC grains[41]. The raw materials used were coarse WC powder with a Fischer particle size of 10 μm and Co powder with a Fischer particle size of 1.5 μm, both produced by Zhuzhou Cemented Carbide Group Corp. Ltd of China.

All samples were prepared by powder technology. According to the set ratio, these powders are wet milled mechanically. The carbon content was fixed to 4.60 wt.% by adding C or W powder. The powder mixtures were milled for 24 h at the ball to powder ratio of 5:1 in ethyl alcohol and dried and granulated. A bars of 25×8×6.7 mm were uniaxially cold pressed under pressure of 100 MPa. The bar samples were sintered at 1410°C under the 6 MPa pressure for 1 h.

In order to study the morphology of WC grains under different carbon contents, the as-sintered sample were re-sintered in a carbon-poor and carbon-rich atmosphere, respectively. One as-sintered sample was buried in the carbon black powders and the other was buried in the alumina powders. These samples were sintered at 1500°C for 6 h again at the same time. Two different samples were obtained, namely carbon-rich sample and carbon-poor sample. In order to observe the morphology of WC grains, the binder phase of the re-sintered sample were removed by immersing in saturation hydrochloric and Fe3Cl mixed solution. Then, the WC grain morphology was observed by scanning electron microscopy (FE-SEM, JSM-6701F, JEOL, Japan).

Acknowledgements

The financial supports from Key R&D program of Science and Technology Department of Jiangxi Province in China (Grant No. S2019ZPYFB1240), National Natural Science Foundation of China (Grant No. 51820105001) and the Special Funds for the Construction of Hunan Innovation Province (Grant no. 2019GK2052) are acknowledged.

References:

1. Exner, H. E. Physical and chemical nature of cemented carbides. *Int. Met. Rev.* **24**, 149-173 (1979).

2. García, J., Collado Ciprés, V., Blomqvist, A. & Kaplan, B. Cemented carbide microstructures: a review. *Int. J. Refract. Met. Hard Mater.* **80**, 40-68 (2019).

3. Norgren, S., Garcia, J., Blomqvist, A. & Yin, L. Trends in the P/M hard metal industry. *Int. J. Refract. Met. Hard Mater.* **48**, 31-45 (2015).

4. Milman, Y. V., Luyckx, S. & Northrop, I. Influence of temperature, grain size and cobalt content on the hardness of WC–Co alloys. *Int. J. Refract. Met. Hard Mater.* **17**, 39-44 (1999).

5. Csanádi, T. *et al.* Deformation characteristics of WC micropillars. *J. Eur. Ceram. Soc.* **34**, 4099-4103 (2014).

6. Delanoë, A. & Lay, S. Evolution of the WC grain shape in WC–Co alloys during sintering: Effect of C content. *Int. J. Refract. Met. Hard Mater.* **27**, 140-148 (2009).

7. Roa, J. J. *et al.* Intrinsic hardness of constitutive phases in WC–Co composites: Nanoindentation testing, statistical analysis, WC crystal orientation effects and flow stress for the constrained metallic binder. *J. Eur. Ceram. Soc.* **35**, 3419-3425 (2015).

8. Nam, H., Lim, J. & Kang, S. Microstructure of (W,Ti)C–Co system containing platelet WC. *Mater. Sci. Eng., A* **527**, 7163-7167 (2010).

9. Yang, Q. *et al.* Fabrication and mechanical properties of WC-10Co cemented carbides with plate-like WC grains. *J. Alloys Compd.* **803**, 860-865 (2019).

10. Bonvalet, M., Odqvist, J., Ågren, J. & Borgenstam, A. Modelling of prismatic grain growth in cemented carbides. *Int. J. Refract. Met. Hard Mater.* **78**, 310-319 (2019).

11. Mannesson, K., Jeppsson, J., Borgenstam, A. & Ågren, J. Carbide grain growth in cemented carbides. *Acta Mater.* **59**, 1912-1923 (2011).

12. Park, Y. J., Hwang, N. M. & Yoon, D. Y. Abnormal growth of faceted (WC) grains in a (Co) liquid matrix. *Metall. Mater. Trans. A* **27**, 2809-2819 (1996).

13. Zhong, Y. & Shaw, L. L. Growth mechanisms of WC in WC–5.75wt% Co. *Ceram. Int.* **37**, 3591-3597 (2011).

14. Ryoo, H. S., Hwang, S. K., Kim, B. K. & Chung, H. S. Anisotropic grain growth based on the atomic adsorption model in WC-25 pct Co alloy. *Metall. Mater. Trans. A* **31**, 1925-1935 (2000).

15. Chen, L.-Q. Phase-Field Models for Microstructure Evolution. *Annu. Rev. Mater. Res.* **32**, 113-140 (2002).

16. Nagashio, K. & Kuribayashi, K. Growth mechanism of twin-related and twin-free facet Si dendrites. *Acta Mater.* **53**, 3021-3029 (2005).

17. Demange, G., Zapolsky, H., Patte, R. & Brunel, M. A phase field model for snow crystal growth in three dimensions. *npj Comput. Mater.* **3**, (2017).

18. Demange, G., Zapolsky, H., Patte, R. & Brunel, M. Growth kinetics and morphology of snowflakes in supersaturated atmosphere using a three-dimensional phase-field model. *Phys. Rev. E* **96**, 022803 (2017).

19. Han, G. M. *et al.* Phase-field modeling of void anisotropic growth behavior in irradiated zirconium. *Comput. Mater. Sci.* **133**, 22-34 (2017).

20. Carlo, A. D., Gurtin, M. E. & Podio-Guidugli, P. A regularized equation for anisotropic motion-by-curvature. *SIAM J. Appl. Math.* **52**, 1111-1119 (1992).

21. Debierre, J. M., Karma, A., Celestini, F. & Guerin, R. Phase-field approach for faceted solidification. *Phys. Rev. E: Stat., Nonlinear, Soft Matter Phys.* **68**, 041604 (2003).

22. Kobayashi, R., Warren, J. A. & Craig Carter, W. A continuum model of grain boundaries. *Phys. D* **140**, 141-150 (2000).

23. Torabi, S., Lowengrub, J., Voigt, A. & Wise, S. A New Phase-Field Model for Strongly Anisotropic Systems. *Proceedings of the Royal Society A Mathematical Physical & Engineering Sciences* **465**, 1337-1359 (2009).

24. Moelans, N., Blanpain, B. & Wollants, P. Quantitative phase-field approach for simulating grain growth in anisotropic systems with arbitrary inclination and misorientation dependence. *Phys. Rev. Lett.* **101**, 025502 (2008).

25. Ribot, J. G., Agrawal, V. & Runnels, B. A new approach for phase field modeling of grain boundaries with strongly nonconvex energy. *Modell. Simul. Mater. Sci. Eng.* **27**, (2019).

26. Zhu, Y. & Hallberg, H. Investigation of faceted void morphologies in UO 2 by phase field modelling. *J. Nucl. Mater.* **467**, 113-120 (2015).

27. Wendler, F., Mennerich, C. & Nestler, B. A phase-field model for polycrystalline thin film growth. *J. Cryst. Growth* **327**, 189-201 (2011).

28. Kobayashi, R. Modeling and numerical simulations of dendritic crystal growth. *Phys. D* **63**, 410-423 (1993).

29. Fleck, M., Mushongera, L., Pilipenko, D., Ankit, K. & Emmerich, H. On phase-field modeling with a highly anisotropic interfacial energy. *Eur. Phys. J. Plus* **126**, (2011).

30. Karma, A. Phase-field formulation for quantitative modeling of alloy solidification. *Phys. Rev. Lett.* **87**, 115701 (2001).

31. Toropova, L. V. *et al.* Theoretical modeling of crystalline symmetry order with dendritic morphology. *Eur. Phys. J.: Spec. Top.* **229**, 275-286 (2020).

32. Eggleston, J. J., McFadden, G. B. & Voorhees, P. W. A phase-field model for highly anisotropic interfacial energy. *Phys. D* **150**, 91-103 (2001).

33. Su, W., Huang, Z., Ren, X., Chen, H. & Ruan, J. Investigation on morphology evolution of coarse grained WC–6Co cemented carbides fabricated by ball milling route and hydrogen reduction route. *Int. J. Refract. Met. Hard Mater.* **56**, 110-117 (2016).

34. Christensen, M., Wahnstrom, G., Allibert, C. & Lay, S. Quantitative analysis of WC grain shape in sintered WC-Co cemented carbides. *Phys. Rev. Lett.* **94**, 066105 (2005).

35. Christensen, M., Wahnstrom, G., Lay, S. & Allibert, C. Morphology of WC grains in WC–Co alloys: Theoretical determination of grain shape. *Acta Mater.* **55**, 1515-1521 (2007).

36. Cheng, K., Zhang, L., Schwarze, C., Steinbach, I. & Du, Y. Phase-field simulation of liquid phase migration in the WC–Co system during liquid phase sintering. *Int. J. Mater. Res.* **107**, 309-314 (2016).

37. Wulff, G. XXV. Zur Frage der Geschwindigkeit des Wachsthums und der Auflösung der Krystallflächen. *Z. Kristallogr.– Cryst. Mater.* **34**, 449 (1901).

38. Hoffman, D. W. & Cahn, J. W. A Vector Thermodynamics for Anisotropic Surfaces I. Fundamentals and Application to Plane Surface Junctions. *Surf. Sci.* **31**, 368-388 (1972).

39. Kim, S., Han, S.-H., Park, J.-K. & Kim, H.-E. Variation of WC grain shape with carbon content in the WC–Co alloys during liquid-phase sintering. *Scripta Mater.* **48**, 635-639 (2003).

40. Sugiyama, I. *et al.* Blunt corners of WC grains induced by lowering carbon content in WC–12mass%Co cemented carbides. *J. Mater. Sci.* **46**, 4413-4419 (2011).

41. Lay, S., Allibert, C. H., Christensen, M. & Wahnström, G. Morphology of WC grains in WC–Co alloys. *Mater. Sci. Eng., A* **486**, 253-261 (2008).